THE JOURNAL OF BIOLOGICAL CHEMISTRY VOL. 290, NO. 18, pp. 11384–11392, May 1, 2015

Structural Basis for the Phosphorylation-regulated Interaction between the Cytoplasmic Tail of Cell Polarity Protein Crumbs and the Actin-binding Protein Moesin*

Received for publication, February 8, 2015, and in revised form, March 16, 2015 Published, JBC Papers in Press, March 19, 2015, DOI 10.1074/jbc.M115.643791

Zhiyi Wei[‡§¶1], **Youjun Li**[‡1], **Fei Ye**[‡§], **and Mingjie Zhang**[‡§2]

From the [‡]*Division of Life Science, State Key Laboratory of Molecular Neuroscience, Hong Kong University of Science and Technology, Clear Water Bay, Kowloon, Hong Kong, China,* [§]*Center of Systems Biology and Human Health, School of Science and Institute for Advanced Study, Hong Kong University of Science and Technology, Clear Water Bay, Kowloon, Hong Kong, China, and* [¶]*Department of Biology, South University of Science and Technology of China, Shenzhen 518055, China*

Background: Crumbs functions in cell growth control via its short cytoplasmic tail.
Results: The structure of the crumbs cytoplasmic tail in complex with moesin protein 4.1/ezrin/radixin/moesin (FERM) domain is determined.
Conclusion: Phosphorylation of crumbs cytoplasmic tail disrupts its binding to moesin but not to protein associated with Lin7–1 (PALS1).
Significance: Our study suggests a model for the role of crumbs in sensing cell growth and apical-basal polarity establishment.

The type I transmembrane protein crumbs (Crb) plays critical roles in the establishment and maintenance of cell polarities in diverse tissues. As such, mutations of *Crb* can cause different forms of cancers. The cell intrinsic role of Crb in cell polarity is governed by its conserved, 37-residue cytoplasmic tail (Crb-CT) via binding to moesin and protein associated with Lin7–1 (PALS1). However, the detailed mechanism governing the Crb·moesin interaction and the balance of Crb in binding to moesin and PALS1 are not well understood. Here we report the 1.5 Å resolution crystal structure of the moesin protein 4.1/ezrin/radixin/moesin (FERM)·Crb-CT complex, revealing that both the canonical FERM binding motif and the postsynaptic density protein-95/Disc large-1/Zonula occludens-1 (PDZ) binding motif of Crb contribute to the Crb·moesin interaction. We further demonstrate that phosphorylation of Crb-CT by atypical protein kinase C (aPKC) disrupts the Crb·moesin association but has no impact on the Crb·PALS1 interaction. The above results indicate that, upon the establishment of the apical-basal polarity in epithelia, apical-localized aPKC can actively prevent the Crb·moesin complex formation and thereby shift Crb to form complex with PALS1 at apical junctions. Therefore, Crb may serve as an aPKC-mediated sensor in coordinating contact-dependent cell growth inhibition in epithelial tissues.

The establishment of epithelial cell polarity is a complicated and dynamic process that involves cell-cell adhesions, assembly of junction complexes, reorganization of cytoskeleton, directional transportation of vesicles, and specific localization of proteins and lipids (1–4). Over the last two decades, genetic and cell biology studies have identified three tripartite protein complexes, namely the crumbs (Crb)[3] complex composed of Crb·PALS1·PALS1-associated tight junction (PATJ), the partition-defective (PAR) complex composed of PAR3/PAR6/aPKC, and the Disc large (DLG) complex composed of DLG/lethal giant larvae (LGL)/Scribble, as the principle cell polarity regulators (5–10). Among these regulators, only Crb is a transmembrane protein and necessary for both the apical-basal cell polarity and the assembly of the zonula adherens in *Drosophila* epithelia (11–13). In early *Drosophila* embryo development, dysfunction mutations of Crb lead to the loss of the apical-membrane identity, and overexpression of Crb causes expansion of the apical-membrane size at the expense of the basolateral membranes (14, 15).

As a type I transmembrane protein, *Drosophila* Crb is composed of an extracellular region, a transmembrane domain, and a 37-residue cytoplasmic tail (Crb-CT) that contains a FERM binding motif (FBM), a PDZ binding motif (PBM), and several potential aPKC phosphorylation sites (16–19) (Fig. 1*A*). Expression of transmembrane domain-tethered Crb-CT alone can rescue most of the embryonic polarity defects in *crb* mutant (15, 16), indicating that the cytoplasmic tail plays a crucial role for the functions of Crb. Mechanistically, the PBM of Crb-CT is known to specifically bind to the PDZ-Src homology 3 (SH3)-guanylate kinase supramodule of PALS1 and stabilizes the apical Crb complex (20), whereas the FBM is considered not to be directly engaged in the polarity complex formation but instead

* This work was supported by Research Grants Council of Hong Kong Grants 663811, 663812, 664113, AoE/M09/12, and T13–607/12R and by the Asia Fund for Cancer Research (to M. Z.).
The atomic coordinates and structure factors (code 4YL8) have been deposited in the Protein Data Bank (http://wwpdb.org/).
[1] Both authors contributed equally to this work.
[2] A Kerry Holdings Professor in Science and a Senior Fellow of the Institute for Advanced Study at HKUST. To whom correspondence should be addressed: Division of Life Science, Hong Kong University of Science and Technology, Clear Water Bay, Kowloon, Hong Kong, China. Tel.: 852-23588709; Fax: 852-23581552; E-mail: mzhang@ust.hk.

[3] The abbreviations used are: Crb, crumbs; FERM, protein 4.1/ezrin/radixin/moesin; aPKC, atypical protein kinase C; PALS1, protein associated with Lin7–1; PDZ, postsynaptic density protein-95/Disc large-1/Zonula occludens-1; CT, cytoplasmic tail; FBM, FERM binding motif; PBM, PDZ-binding motif; ERM, ezrin/radixin/moesin; ITC, isothermal titration calorimetry; PIP_2, phosphatidylinositol 4,5-bisphosphate.

to be involved in the Hippo signaling pathway and the apical membrane-cytoskeleton regulations (21–25). Coincidently, the aPKC phosphorylation sites in Crb-CT are located near or within the Crb-FBM (Fig. 1*A*), implying that the interaction(s) between Crb-FBM and its target(s) may be regulated by aPKC-mediated phosphorylation of Crb-CT.

The ezrin-radixin-moesin (ERM) proteins are a family of widely distributed membrane-associated proteins that provide a structural linkage between plasma membranes and cortical cytoskeletons (26–30). These three proteins share similar domain organizations and high sequence identities, all having an N-terminal FERM domain and a C-terminal domain that can fold back to bind to the FERM domain forming an autoinhibited conformation (Fig. 1*A*) (31–33). The autoinhibited ERMs can be activated by phosphorylation on a conserved Thr (Thr-567 in ezrin, Thr-564 in radixin, Thr-558 in moesin) at their respective inhibitory C-terminal domain and/or via binding to phosphatidylinositol 4,5-bisphosphate (PIP_2) (34–37). The activated ERMs then bind to membranes via their FERM domains (directly to membrane lipids and/or transmembrane proteins) and to actin filaments via their C-terminal actin binding motifs. In *Drosophila* epithelia, Crb exhibits close co-localization with moesin and stabilizes the apical membrane-cytoskeleton, leading to reinforcement of the zonula adherens and effective coupling between epithelial morphogenesis and cell polarity (25). However, the detailed mechanism governing the Crb·moesin interaction and Crb-mediated regulation between apical-basal cell polarity and apical cytoskeleton reorganization are not well understood.

Here we biochemically and structurally characterized the interaction between Crb-CT and moesin FERM domain. The 1.5 Å resolution crystal structure of the moesin-FERM·Crb-CT complex reveals a typical FERM/FBM binding mode in which the FBM of Crb-CT forms a short β-strand and fits into the canonical F3 lobe target binding site. To our surprise, the PBM of Crb-CT also contributes to the binding to moesin-FERM by occupying the PIP_2 binding site at the F1/F3 cleft, implying that Crb-CT may mimic the role of PIP_2 in the activation of the ERM family proteins. We further show by NMR spectroscopy that phosphorylation of Crb-CT by aPKC disrupts the Crb·moesin association, likely by preventing the formation of the β-strand conformation of the Crb-FBM. The biological implications of these findings are discussed.

EXPERIMENTAL PROCEDURES

Protein Expression and Purification—The mouse moesin FERM domain (residues 1–297) and fly Crb-CT (residues 2110–2146) were amplified by PCR using their respective full-length cDNA as the templates. Each PCR product was individually cloned into a modified pET-32 M vector. Various mutants were created using standard two-step PCR-based methods and confirmed by DNA sequencing. Recombinant proteins each with an N-terminal Trx-His_6 tag were expressed in *Escherichia coli* BL21(DE3) cells at 16 °C. The expressed proteins were purified by a nickel-nitrilotriacetic acid-agarose affinity chromatography followed by a size-exclusion chromatography.

Isothermal Titration Calorimetry (ITC) Assay—ITC was carried out on a MicroCal VP-ITC at 25 °C. All proteins were dissolved in a buffer containing 50 mM Tris, pH 7.5, 400 mM NaCl, 1 mM EDTA, and 1 mM DTT. The titration processes were performed by injecting 5–10-μl aliquots of protein samples in a syringe (concentration of 200 μM) into protein samples in cell (concentration of 20 μM) at time intervals of 120 s to ensure that the titration peak returned to the baseline. The relatively high salt concentration is used to ensure that the FERM domains used in the binding studies behave well in solution. The data were analyzed using the Origin 7.0 program and fitted by the one-site binding model.

Nuclear Magnetic Resonance (NMR) Spectroscopy—NMR samples containing 1.5 mM Crb-FBM (^{2111}NKRATRGTYSPSAQE^{2125}) or Crb-FBM_Thr(P)-2118 peptide were dissolved in 50 mM potassium phosphate, pH 6.5, with 90% H_2O, 10% D_2O. NMR spectra were acquired at 283 K on a Varian Inova 750-MHz spectrometer. Mixing times of 300 and 75 ms were used for the nuclear Overhauser effect spectroscopy (NOESY) and total correlated spectroscopy (TOCSY) experiments, respectively. Spectra were processed using NMRPipe (38) and analyzed with Sparky software.

Crystallization—For crystallization, the tagged proteins were treated with a small amount of human rhinovirus 3C protease at 4 °C overnight to cleave the fusion tags and further purified by a step of size-exclusion chromatography. Crystals of the Moesin-FERM·Crb-CT complex were obtained by the hanging drop vapor diffusion method at 16 °C within 2 days. To set up a hanging drop, 1 μl of concentrated protein mixture at a 1:1 stoichiometric ratio was mixed with 1 μl of crystallization solution with 20% PEG3350 and 0.2 M ammonium iodine. Before diffraction experiments, crystals were soaked in the crystallization solution containing an additional 30% glycerol for cryoprotection. The diffraction data were collected at the Shanghai Synchrotron Radiation Facility and were processed and scaled using HKL2000 (39).

Structure Determination—The initial phase was determined by molecular replacement using the apo form of moesin-FERM (PDB code 1EF1) as the searching model. The model was refined in Phenix (40) against the 1.5 Å dataset. The Crb-CT peptide was built subsequently in COOT (41). In the final stage, an additional TLS refinement was performed in Phenix. The final model was further validated by using MolProbity (42). The refinement statistics are listed in Table 1. All structure figures were prepared using PyMOL. The sequence alignments were prepared and presented using ClustalW (43).

RESULTS

Crb-CT Specifically Binds to Moesin FERM Domain—Unlike its extracellular region, the Crb-CT, especially the PBM, FBM, and aPKC phosphorylation sites, is highly conserved across different species and isoforms (Fig. 1*A*). Specifically, the fly Crb-CT is essentially the same as mammalian Crb2-CT, and therefore, we continued to use the fly Crb-CT after our recent study of the Crb-CT/PALS1 interaction (20). To investigate the Crb·moesin interaction, we used highly purified recombinant Crb-CT and moesin-FERM proteins. Quantitative binding assays showed that Crb-CT directly binds to moesin-FERM with a disassociation constant (K_d) of ~5 μM in the presence of 400 mM NaCl in the assayed buffer (Fig. 1*B*). Interestingly,

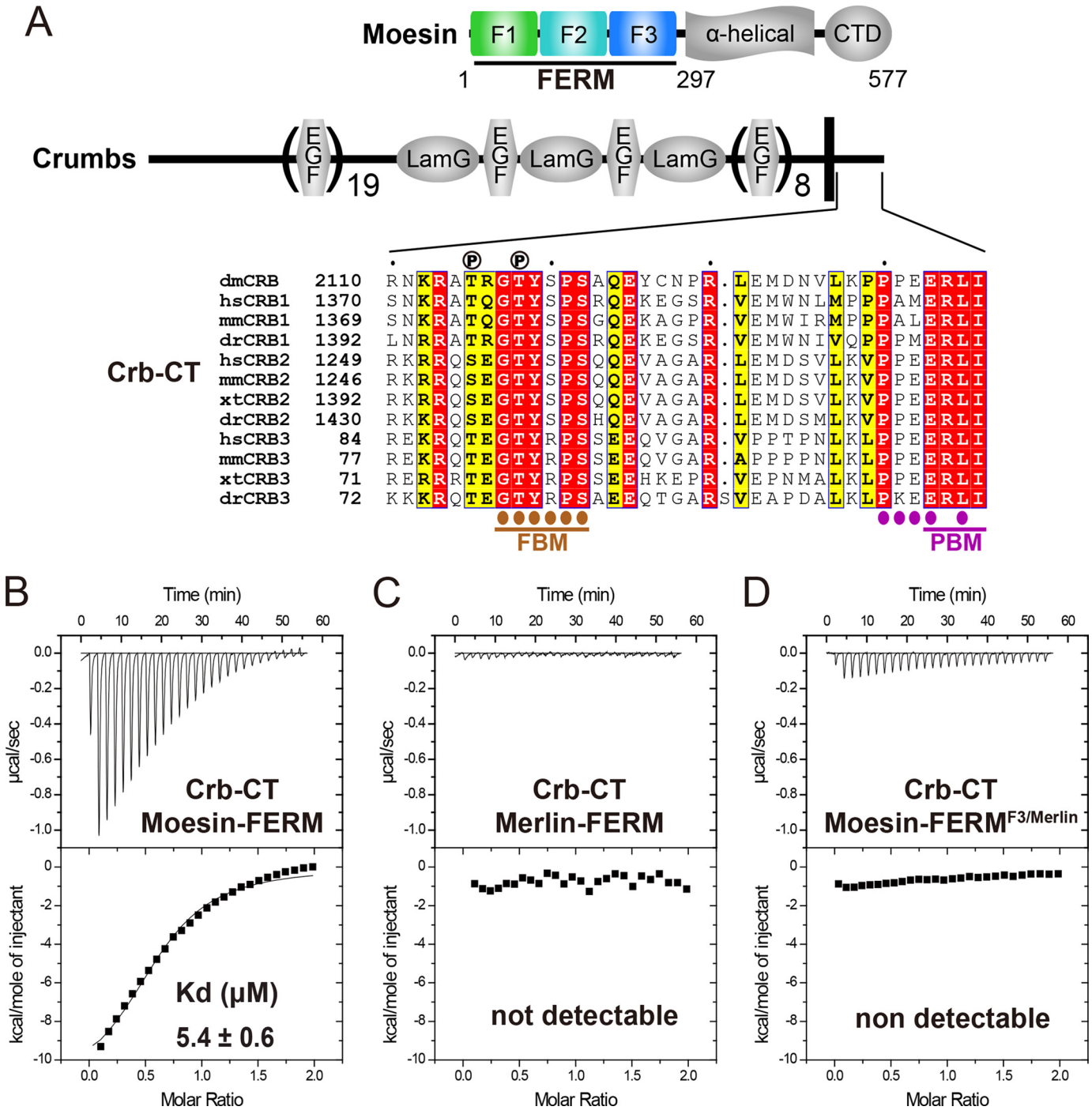

FIGURE 1. **Crb-CT specifically binds to moesin-FERM.** *A*, schematic diagram showing the domain organization of moesin and Crb and the amino acid sequence alignment of the cytoplasmic tails of different Crb proteins (*hs* for human, *mm* for mouse, *xt* for *Xenopus tropicalis*, *dr* for *Danio rerio*, and *dm* for *Drosophila melanogaster*). In this alignment, residues that are absolutely conserved and highly conserved are highlighted in *red* and *yellow*, respectively. The residues involved in the FERM/FBM and FERM/PBM interactions are indicated by *brown* and *purple circles*, respectively. The potential phosphorylation sites by aPKC are labeled *above the alignment*. *Lam G*, laminin G domain; *CTD*, C-terminal domain. *B–D*, ITC-based measurements showing the binding profiles of Crb-CT to moesin-FERM (*B*), Merlin-FERM (*C*), and moesin-FERM$^{F3/Merlin}$ (*D*), respectively.

although sharing a high amino acid sequence identity with moesin-FERM, the FERM domain of merlin had no detectable binding to Crb-CT (Fig. 1*C*), indicating that moesin-FERM encodes its intrinsic target binding specificity. A moesin-FERM chimera (termed as moesin-FERM$^{F3/Merlin}$), in which the F3 lobe was replaced by the corresponding F3 lobe of merlin, failed to bind to Crb-CT (Fig. 1*D*), indicating that the F3 lobe is chiefly responsible for the binding of moesin-FERM to Crb-CT.

Overall Structure of the Moesin-FERM·Crb-CT Complex—To understand the molecular basis governing the moesin·Crb interaction, we determined the structure of moesin-FERM in complex with Crb-CT by x-ray crystallography (Table 1). The moesin-FERM·Crb-CT complex crystals were diffracted to up to 1.5 Å resolution. In the crystals the moesin-FERM·Crb-CT complex forms a heterodimer with one complex per asymmetric unit. The final structural model contains most of residues

TABLE 1
Statistics of data collection and model refinement
Numbers in parentheses represent the value for the highest resolution shell.

Data collection	
Space group	$P2_12_12_1$
Unit cell parameters (Å)	$a = 63.2$, $b = 65.2$, $c = 83.4$
Resolution range (Å)	50-1.5 (1.53-1.5)
No. of unique reflections	55,529 (2,724)
Redundancy	7.2 (7.3)
I/σ	33.5 (3.5)
Completeness (%)	99.8 (100)
R_{merge} (%)[a]	6.5 (65.8)
Structure refinement	
Resolution (Å)	50-1.5 (1.54-1.5)
R_{cryst}[b]/R_{free} (%)[c]	15.9 (21.4)/19.1 (26.6)
r.m.s.d bonds (Å)/angles (°)	0.006/1.05
Average B factor	24.6
No. of atoms	
Protein atoms	2,748
Water molecules	268
Other molecules	28
No. of reflections	
Working set	53,440
Test set	1,994
Ramachandranplot[d]	
Favored regions (%)	98.5
Allowed regions (%)	1.5
Outliner (%)	0.0

[a] $R_{merge} = \sum I_i - I_m|/\sum I_i$, where I_i is the intensity of the measured reflection, and I_m is the mean intensity of all symmetry related reflections.
[b] $R_{cryst} = \Sigma||F_{obs}| - |F_{calc}||/\Sigma|F_{obs}|$, where F_{obs} and F_{calc} are observed and calculated structure factors.
[c] $R_{free} = \Sigma_T||F_{obs}| - |F_{calc}||/\Sigma_T|F_{obs}|$, where T is a test data set of ~3.6% of the total reflections randomly chosen and set aside prior to refinement.
[d] Defined by MolProbity.

from the complex, except for a flexible loop (residues 2127–2135) of Crb-CT, which connects its FBM and PBM (Fig. 1*A* and Fig. 2). Moesin-FERM adopts a typical cloverleaf architecture composed of three lobes (F1, F2, and F3). The overall fold of the FERM domain in the moesin·Crb complex structure is essentially identical to the apo moesin-FERM structure (the overall RMSD of 1.6 Å with the 285 aligned residues). The two highly conserved motifs in Crb-CT, FBM and PBM, bind to moesin-FERM at the F3 lobe and a cleft between the F1 and F3 lobes, respectively (Fig. 2).

The Crb-FBM Binding Site in the F3 Lobe of Moesin-FERM—In FERM-containing proteins, F3 lobes act as the major target binding site. A groove (known as the $\alpha\beta$-groove) mainly formed by $\beta5_{F3}$ and $\alpha1_{F3}$ is a well characterized target binding region in FERM domains including those of moesin (44), radixin (45–48), talin (49, 50), Merlin (51), and myosin-X (52, 53). Most of the previously characterized targets, especially those interacting with ERM proteins, bind to the $\alpha\beta$-groove in a β-strand or β-strand-like structures (Fig. 3*B*). In the moesin-FERM·Crb-CT complex, the FBM of Crb also adopts a β-strand structure and binds to the $\alpha\beta$-groove in the F3 lobe of moesin-FERM (Fig. 3*A*), extending the anti-parallel β-sheet formed by $\beta5_{F3}$, $\beta6_{F3}$, and $\beta7_{F3}$. The FBM/F3 interaction is mainly mediated by hydrogen bonds. Some hydrophobic interactions (*e.g.* Pro-2121_{Crb} inserts its aliphatic side chain into a hydrophobic cleft formed by Ile-245_{F3} and Ile-248_{F3}) also contribute to the FBM/F3 interaction. The three consecutive and strictly conserved residues in the FBM, Gly-2117, Thr-2118, and Tyr-2119 (termed as the GTY motif and known as the iconic sequence of FBMs), are intimately involved in the FBM/F3 interaction (Fig. 3*A*). The very tight packing between Gly-2117 and the ring of Phe-250_{F3} is afforded by the lack of side chain of Gly-2117. The

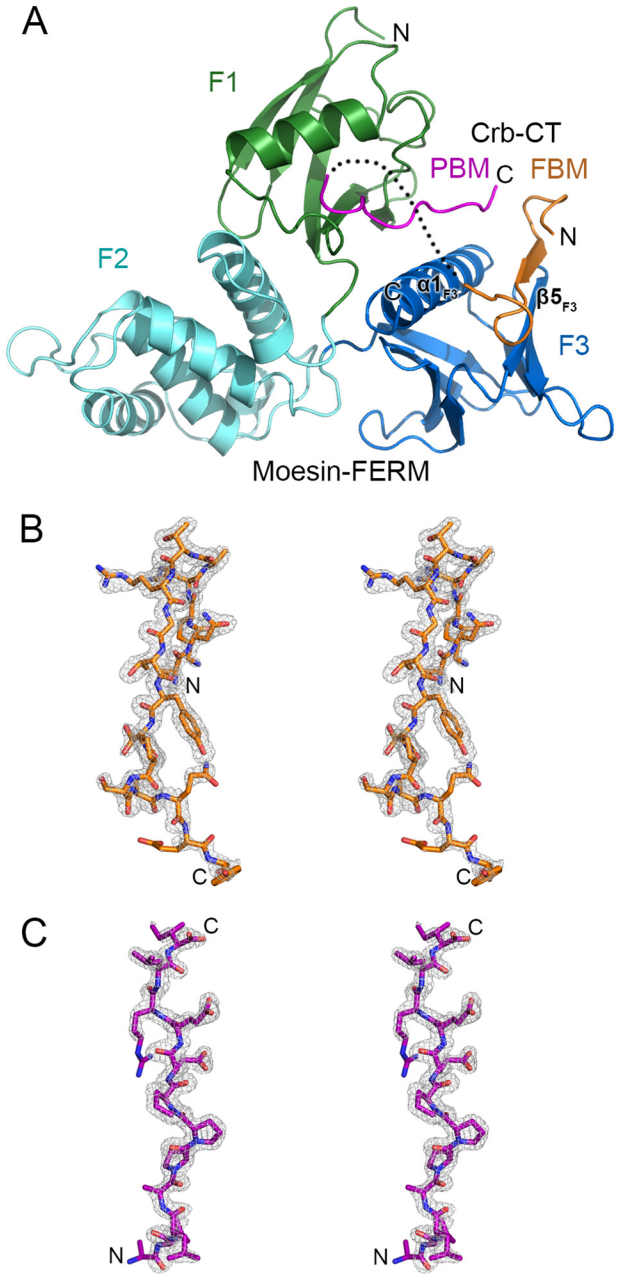

FIGURE 2. **Overall structure of the moesin-FERM·Crb-CT complex.** *A*, the ribbon diagram structure of moesin-FERM·Crb-CT complex with the three lobes of moesin-FERM, F1 (*green*), F2 (*cyan*), and F3 (*blue*), Crb-FBM (*gold*), and Crb-PBM (*purple*) drawn in their specific colors. The same color code is used throughout the rest of the paper except as otherwise indicated. The disordered loop connecting the FBM and PBM is indicated by a *dotted line*. *B* and *C*, the electron-density maps (countered at 1σ) of the FBM and PBM in the complex are shown in *B* and *C*, respectively, with their respective stick models overlapped.

side chain of Thr-2118 forms a pair of hydrogen bonds with Asp-247_{F3}. Tyr-2119 forms a strong hydrogen bond with His-288_{F3} (bond length of 2.7 Å) in addition to interacting with Met-285_{F3} through their hydrophobic side chains. Consistent with our structural analysis, the substitution of Tyr-2119 with Ala abolished Crb-CT binding to moesin-FERM (Fig. 3*C*).

The PBM of Crb Binds to the F1/F3 Cleft of Moesin-FERM—An unexpected finding in the moesin·Crb complex structure is that the Crb-PBM directly contacts the moesin FERM domain

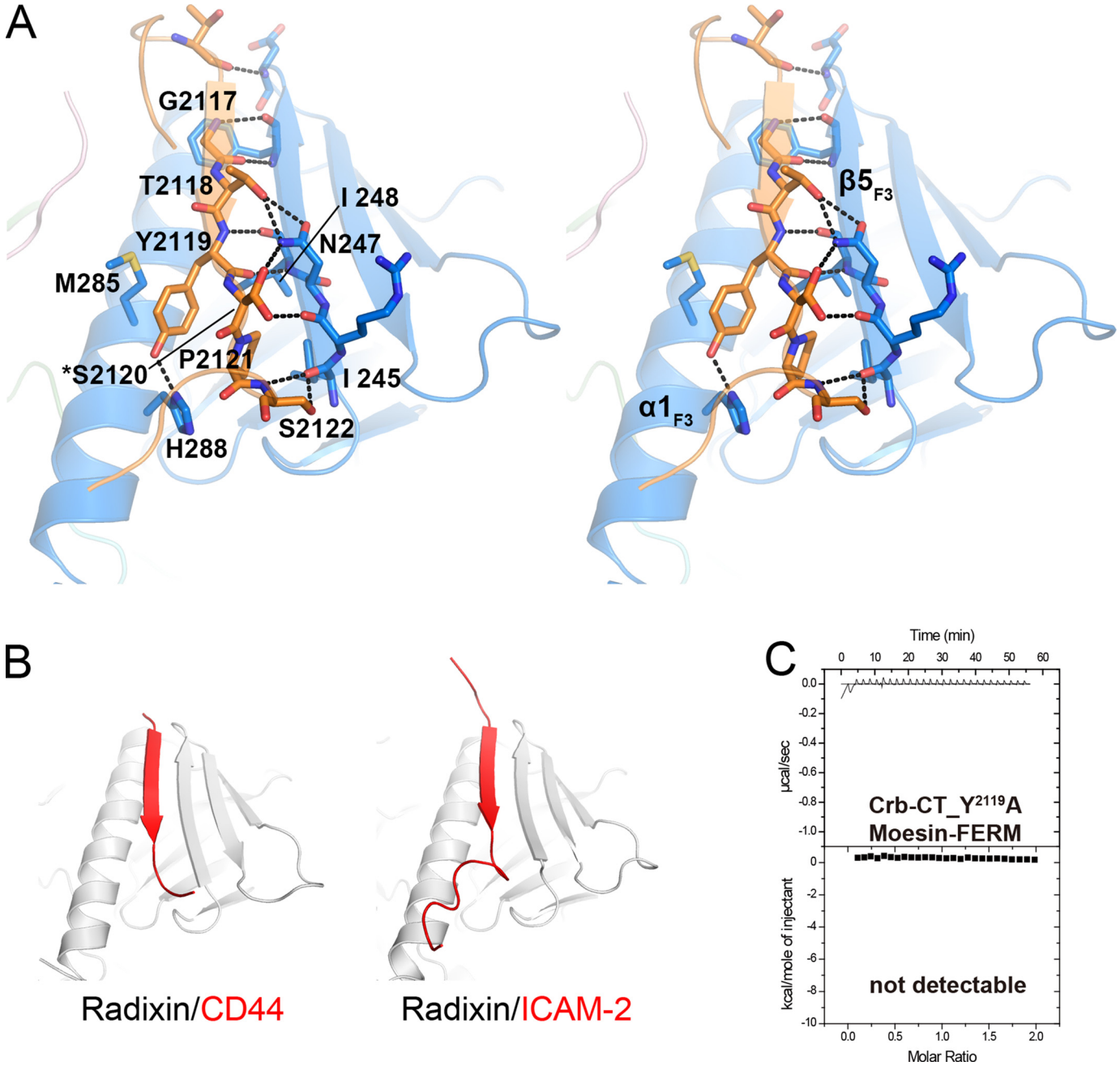

FIGURE 3. **The moesin-FERM/Crb-FBM interaction.** *A*, a stereo view of the molecular details of the moesin-FERM/Crb-FBM interaction. Notably, Ser-2120 at the Crb-CT adopts a dual-conformation. Hydrogen bonds are indicated by *dashed lines*. *B*, two examples showing that previously characterized targets (CD44 and ICAM-2) bind to the $\alpha\beta$-groove in the F3 lobe of radixin (another ERM protein) as a β-strand. *C*, ITC-based assay showing that the Crb-CT_Y2119A mutant displays no detectable binding to moesin-FERM.

(Fig. 2*A*), a mode that has not been observed in any other FERM domains characterized biochemically and structurally. The last seven residues of Crb-CT, which contains its PBM, fit snuggly into the cleft formed by highly conserved residues from the F1 and F3 lobes (Fig. 4*A*). The C-terminal tail carboxyl group of Crb-PBM forms a salt bridge with Lys-278_{F3}. Leu-2145_{Crb} at the -1 position of PBM inserts into a hydrophobic pocket formed by Leu-281_{F3}, Phe-250_{F3}, and the aliphatic part of Lys-278_{F3}. Glu-2143_{Crb} at the -3 position of PBM forms two salt bridges with Lys-60_{F1} and Lys-83_{F1}. The residues immediately N-terminal to Crb-PBM also play a role in binding to the F1/F3 cleft (Fig. 4*A*). Glu-2142_{Crb} makes two hydrogen bonds with the main chains of Leu-61 and Asn-62 in the $\beta4/\beta5$ loop of the F1 lobe. The two proline residues, Pro-2140_{Crb} and Pro-2141_{Crb}, are involved in hydrophobic interactions with residues from the F1 and F3 lobes. Consistent with the above structural analysis, removal of the last four residues from Crb-CT weakened its binding to moesin-FERM by ~5-fold assayed in high salt buffers (Fig. 4*B*). We expect that the contribution of the PBM to the Crb-CT/moesin-FERM is larger at physiological salt concentrations, given the heavy involvement of the charged residues in the interaction. It is important to note that the residues involved in the moesin-FERM·Crb-CT interaction are highly conserved in ERM proteins as well as Crb homologs across spe-

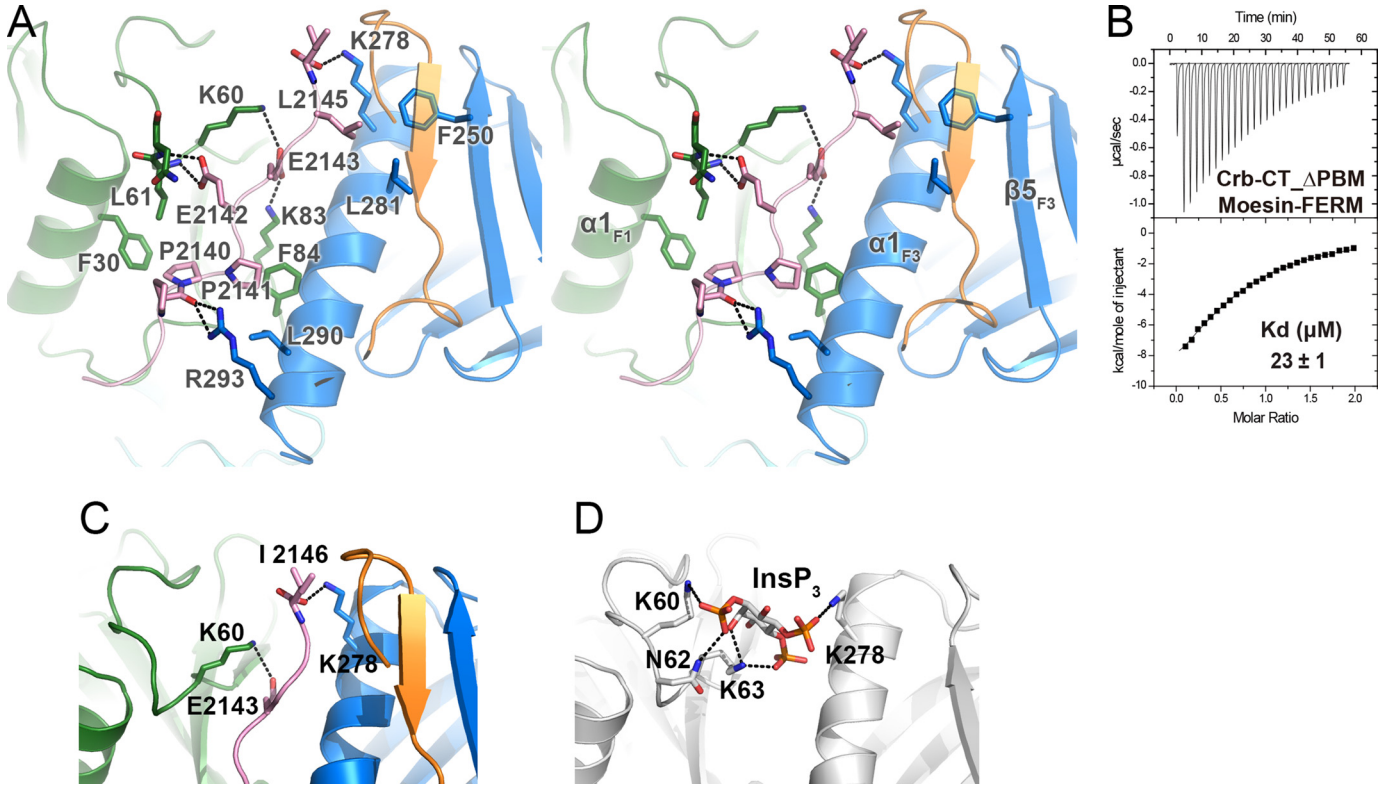

FIGURE 4. **The moesin-FERM/Crb-PBM interaction.** *A*, a stereo view of the molecular details of the moesin-FERM/Crb-PBM interaction. *B*, ITC-based measurement displaying the interaction between Crb-CT-ΔPBM and moesin-FERM. *C* and *D*, comparison of the bindings of Crb-PBM and inositol 1,4,5-trisphosphate ($InsP_3$)to the cleft in the F1/F3 interface of moesin-FERM. Note that the extreme tail carboxyl group and the carboxyl group of Glu2143 of Crb-PBM mimic the phosphate groups of phosphatidylinositol 1,4,5-phosphate in binding to positively charged residues of moesin-FERM.

cies (Fig. 1*A*), suggesting that this interaction is conserved throughout metazoan.

ERM proteins are believed to associate with membranes either by binding to transmembrane proteins or directly to phospholipids. The association of ERMs with PIP_2 potentiates the activation of ERM proteins (34, 37). Interestingly, the Crb-PBM binding site in F1/F3 cleft overlaps with the PIP_2 head group binding site on moesin-FERM (54) and the Crb-PBM mimics PIP_2 binding to moesin by engaging positively charged residues in the F1/F3 cleft (Fig. 4, *C* and *D*), indicating that the bindings of Crb and PIP_2 to moesin-FERM are mutually exclusive. Therefore, it is hypothesized that the association of Crb with ERMs may potentiate the activation as well as membrane localization of ERMs better than phospholipids alone.

aPKC Phosphorylates Crb and in Turn Abolishes the Moesin·CrbInteraction—AlthoughaPKC-dependentphosphorylation of Crb is essential for epithelial apical-basal cell polarity in *Drosophila* (19), the molecular basis underlying this phosphorylation-dependent cell polarity establishment and maintenance is not clear. The aPKC phosphorylation sites (Thr-2115 and Thr-2118) are located near/in Crb-FBM (Fig. 3*A*). We demonstrated earlier on that Crb-FBM is not involved in the binding of Crb-CT to PALS1 (20). Therefore, we focused our investigation on the potential phosphorylation-regulated interaction between Crb-CT and moesin-FERM. Perhaps it is not too surprising that a phosphorylation-mimic mutation of Crb-CT (Crb-CT_T2118E) only moderately weakened its binding to moesin-FERM (Fig. 5*A*), as the side chain of Thr-2118 is solvent-exposed and makes relatively minor contribution to the binding by forming hydrogen bond with $Asp\text{-}247_{F3}$. Surprisingly, a synthetic phosphor-peptide of Crb-CT, in which Thr-2118 of the FBM (*i.e.* GT2118Y) was specifically phosphorylated, displayed no detectable binding to moesin-FERM (Fig. 5*B*), indicating that aPKC-mediated phosphorylation can completely disrupt the Crb·moesin interaction. Based on the structure shown in Fig. 3*A*, the large difference between the phosphor-mimetic mutation of Crb-CT (Crb-CT_T2118E) and the corresponding phosphor-Crb-CT (Crb-CT_Thr(P)-2118) in their bindings to moesin-FERM cannot be explained solely by their charge differences. Instead, the phosphorylation of Thr-2118 might alter the conformation of Crb-CT, and such phosphorylation-induced conformational alterations cannot be fully mimicked by the T2118E mutation. To test this hypothesis, we compared the structural changes of Crb-CT induced by Thr-2118 phosphorylation by NMR spectroscopy. The NOE pattern of WT Crb-FBM peptide derived from the ^1H homonuclear NOESY spectrum indicates that the peptide adopts a largely extended structure (Fig. 5*D*) and thus can easily form the observed β-strand structure upon forming complex with moesin-FERM. In contrast, a stretch of (i, i+2) NOEs surrounding Thr(P)-2118 were detected for the Crb-FBM_Thr(P)-2118 peptide (Fig. 5, *E* and *F*), indicating that phosphorylation of Thr-2118 induces the formation of a turn-like structure between Arg-2116 and Ser-2120, and this turn-like structure is likely stabilized by the interaction of the side chains between Arg-2116 and Thr(P)-2118 (Fig. 5, *E* and *F*). As a consequence, the

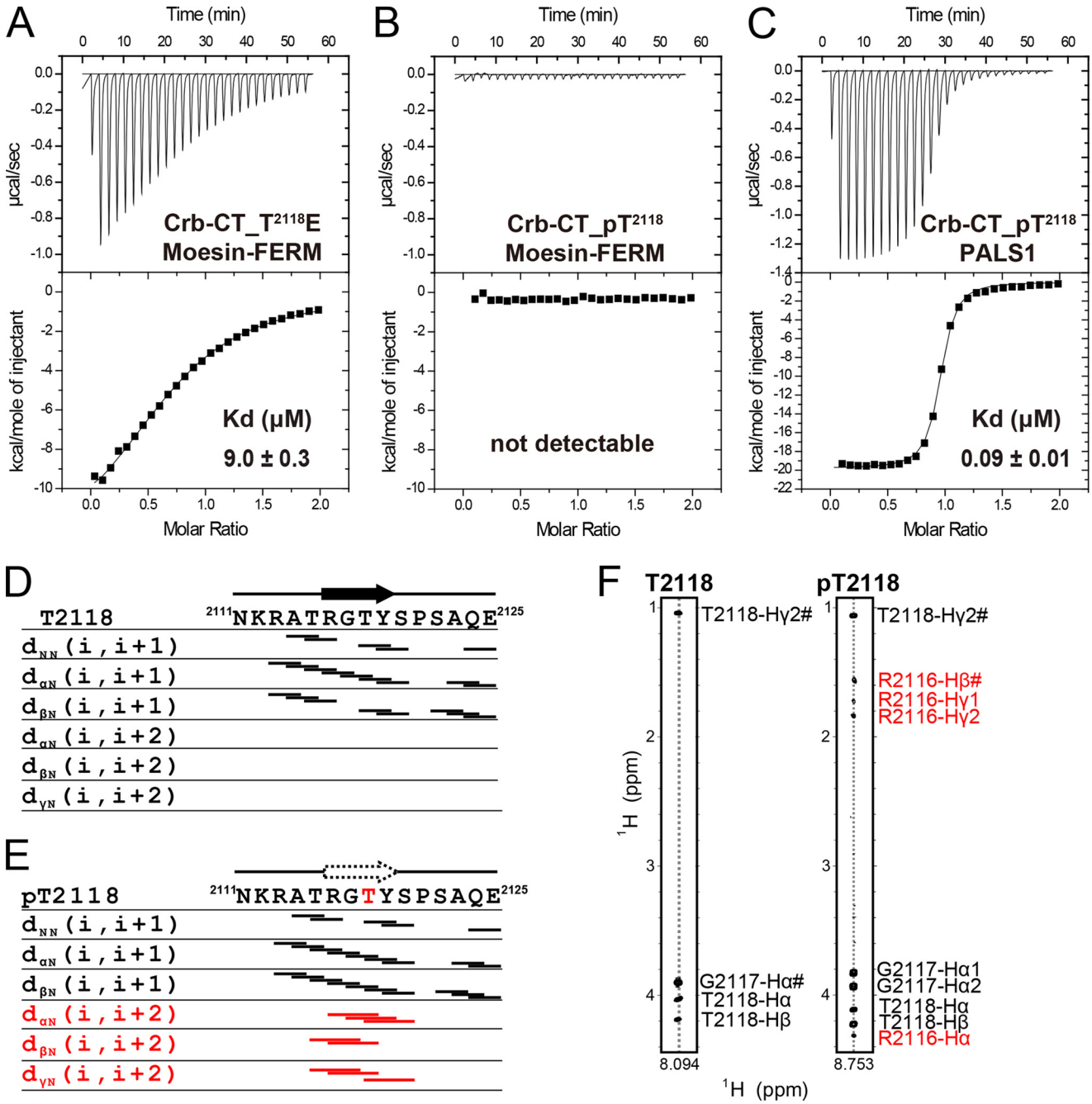

FIGURE 5. **Phosphorylation of Thr-2118 abolishes the moesin·Crb interaction.** *A–C*, ITC-based measurements showing the binding profiles between Crb-CT_T2118E (*A*) or Crb-CT_Thr(P)-2118 (*B*) and moesin-FERM and between Crb-CT_Thr(P)-2118 and PALS1 PDZ-SH3-GK (*C*). *D* and *E*, NMR analysis comparing the short and medium ranged NOE patterns of the Crb-FBM and the Crb-FBM_Thr(P)-2118 peptides. The specific medium-range i to i+2 NOEs detected from Arg-2116 to Thr(P)-2118 in the Crb-FBM_Thr(P)-2118 peptide (colored in *red*) indicates formation of a turn-like structure in this region. *F*, a selected region of ^{1}H two-dimensional NOESY spectrum of Crb-FBM peptide (*left*) and that of Crb-FBM_Thr(P)-2118 peptide (*right*) showing the NOE peaks of amide proton of Thr-2118 and Thr(P)-2118, respectively.

formation of the turn-like structure of the phosphor-Crb-FBM likely prevents Crb-CT from binding to moesin-FERM.

DISCUSSION

The interaction between Crb-CT and moesin characterized here is ~50-fold weaker than the Crb-CT/PALS1 interaction that we demonstrated earlier on (20). Would the crumbs·moesin interaction even occur if PALS1 is present? We believe that both interactions can exist in cells, but the two interactions likely occur in different regions/time points/growth conditions in living cells. There are several possible scenarios that can occur in cells. Although the binding between crumbs and moesin is not very strong, the enrichment of moesin by actin filaments (via the C-terminal actin binding domain of moesin) can increase the binding avidity between crumbs and moesin. In polarized epithelial cells, PALS1 is normally enriched in the apical cell cortex together with aPKC; the PALS1/crumbs interaction would dominate under such condition. On the other

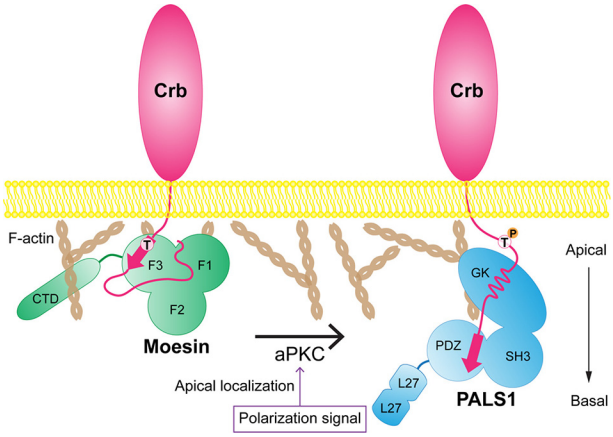

FIGURE 6. **A model showing aPKC-induced shift of Crb from the moesin complex to the PALS1 complex.** In this model the establishment of the apical-basal polarity leads to apical enrichment and activation of aPKC and subsequent phosphorylation of Crb-FBM. The phosphorylation of Crb-FBM weakens its binding to moesin-FERM, which in turn promotes Crb to form complex with PALS1 and subsequent stabilization of the apical-basal polarity. *SH3*, Src homology 3; *GK*, guanylate kinase; *CTD*, C-terminal domain; *L27*, Lin-2/Lin-7.

hand, the moesin/crumbs complex may have the advantage of forming in regions with enriched moesin/actin filaments (*e.g.* at leading edges of non-polarized migrating cells).

Actin cytoskeleton reorganization is a major step during the establishment of apical-basal cell polarity. A series of recent studies has shown that the actin cytoskeleton organization is closely linked to the Hippo signaling pathway, as numerous Hippo-mediated cellular processes (*e.g.* cell growth and differentiation, cell-cell, and cell-matrix contact-induced tissue morphogenesis/homeostasis, cell migrations, etc.) involve changes in the F-actin structures (55–60). We demonstrate in this study that aPKC-mediated phosphorylation of Crb-CT disrupts its binding to moesin and thus can result in weakening of the moesin-tethered coupling of Crb-harboring plasma membranes to cortical actin cytoskeleton and consequent reduction of cortical tensions in polarized epithelia. This cortical tension change may then trigger the activation of the Hippo signaling pathway and prevent cells from further growth. Because aPKC-mediated phosphorylation of Crb-CT does not affect the interaction between Crb-CT and PALS1 (Fig. 5*C*), aPKC phosphorylation-mediated release of Crb from moesin is likely to be accompanied by increased formation of the Crb·PALS1 complex at the tight junctions, a process favorable for cell polarity establishment and stabilization. As such, a plausible picture of the role of Crb in connecting apical-basal cell polarity establishment and contact-induced cell growth inhibition emerges (Fig. 6). In this picture, formation of the apical-basal polarity leads to apical enrichment and activation of aPKC and subsequent phosphorylation of Crb-CT. The phosphorylated Crb dissociates from moesin and in turn promotes Crb to form complex with PALS1, thereby stabilizing apical-basal polarity with concomitant cell growth inhibition possibly via activation of the Hippo signaling pathway. In addition to its role in the regulation of apical-basal cell polarity and apical membrane/cytoskeleton interactions, Crb-CT has also been reported to directly function in the Hippo signaling pathway by binding to the FERM domain-containing protein Expanded (22, 23). Both Crb/Expanded and Crb·moesin interactions involve the conserved FBM with aPKC phosphorylation sites. Understanding the relations of Crb-CT to its diverse targets may provide further insights for the regulatory roles of Crb in distinct cellular processes. Our study here indicates that aPKC plays a vital regulatory role in determining the functions of Crb in cell growth or cell polarity establishment.

Acknowledgment—We thank the Shanghai Synchrotron Radiation Facility (SSRF) BL17U for x-ray beam time.

REFERENCES

1. Martin-Belmonte, F., and Perez-Moreno, M. (2012) Epithelial cell polarity, stem cells, and cancer. *Nat. Rev. Cancer* **12,** 23–38
2. Rodriguez-Boulan, E., and Macara, I. G. (2014) Organization and execution of the epithelial polarity programme. *Nat. Rev. Mol. Cell Biol.* **15,** 225–242
3. Tepass, U. (2012) The apical polarity protein network in *Drosophila* epithelial cells: regulation of polarity, junctions, morphogenesis, cell growth, and survival. *Annu. Rev. Cell Dev. Biol.* **28,** 655–685
4. Margolis, B., and Borg, J. P. (2005) Apicobasal polarity complexes. *J. Cell Sci.* **118,** 5157–5159
5. Bulgakova, N. A., and Knust, E. (2009) The Crumbs complex: from epithelial-cell polarity to retinal degeneration. *J. Cell Sci.* **122,** 2587–2596
6. Knust, E., and Bossinger, O. (2002) Composition and formation of intercellular junctions in epithelial cells. *Science* **298,** 1955–1959
7. Nance, J., and Zallen, J. A. (2011) Elaborating polarity: PAR proteins and the cytoskeleton. *Development* **138,** 799–809
8. Suzuki, A., and Ohno, S. (2006) The PAR-aPKC system: lessons in polarity. *J. Cell Sci.* **119,** 979–987
9. Tepass, U., Tanentzapf, G., Ward, R., and Fehon, R. (2001) Epithelial cell polarity and cell junctions in *Drosophila*. *Annu. Rev. Genet.* **35,** 747–784
10. Bilder, D. (2004) Epithelial polarity and proliferation control: links from the *Drosophila* neoplastic tumor suppressors. *Genes Dev.* **18,** 1909–1925
11. Pocha, S. M., and Knust, E. (2013) Complexities of Crumbs function and regulation in tissue morphogenesis. *Curr. Biol.* **23,** R289–R293
12. Tepass, U. (1996) Crumbs, a component of the apical membrane, is required for zonula adherens formation in primary epithelia of *Drosophila*. *Dev. Biol.* **177,** 217–225
13. Tepass, U., Theres, C., and Knust, E. (1990) Crumbs encodes an EGF-like protein expressed on apical membranes of *Drosophila* epithelial cells and required for organization of epithelia. *Cell* **61,** 787–799
14. Wodarz, A., Grawe, F., and Knust, E. (1993) CRUMBS is involved in the control of apical protein targeting during *Drosophila* epithelial development. *Mech. Dev.* **44,** 175–187
15. Wodarz, A., Hinz, U., Engelbert, M., and Knust, E. (1995) Expression of crumbs confers apical character on plasma membrane domains of ectodermal epithelia of *Drosophila*. *Cell* **82,** 67–76
16. Klebes, A., and Knust, E. (2000) A conserved motif in Crumbs is required for E-cadherin localisation and zonula adherens formation in *Drosophila*. *Curr. Biol.* **10,** 76–85
17. Klose, S., Flores-Benitez, D., Riedel, F., and Knust, E. (2013) Fosmid-based structure-function analysis reveals functionally distinct domains in the cytoplasmic domain of *Drosophila* crumbs. *G3* **3,** 153–165
18. Laprise, P., Beronja, S., Silva-Gagliardi, N. F., Pellikka, M., Jensen, A. M., McGlade, C. J., and Tepass, U. (2006) The FERM protein Yurt is a negative regulatory component of the crumbs complex that controls epithelial polarity and apical membrane size. *Dev. Cell* **11,** 363–374
19. Sotillos, S., Díaz-Meco, M. T., Caminero, E., Moscat, J., and Campuzano, S. (2004) DaPKC-dependent phosphorylation of Crumbs is required for epithelial cell polarity in *Drosophila*. *J. Cell Biol.* **166,** 549–557
20. Li, Y., Wei, Z., Yan, Y., Wan, Q., Du, Q., and Zhang, M. (2014) Structure of Crumbs tail in complex with the PALS1 PDZ-SH3-GK tandem reveals a highly specific assembly mechanism for the apical Crumbs complex. *Proc. Natl. Acad. Sci. U.S.A.* **111,** 17444–17449

21. Chen, C. L., Gajewski, K. M., Hamaratoglu, F., Bossuyt, W., Sansores-Garcia, L., Tao, C., and Halder, G. (2010) The apical-basal cell polarity determinant Crumbs regulates Hippo signaling in *Drosophila*. *Proc. Natl. Acad. Sci. U.S.A.* **107,** 15810–15815
22. Ling, C., Zheng, Y., Yin, F., Yu, J., Huang, J., Hong, Y., Wu, S., and Pan, D. (2010) The apical transmembrane protein Crumbs functions as a tumor suppressor that regulates Hippo signaling by binding to Expanded. *Proc. Natl. Acad. Sci. U.S.A.* **107,** 10532–10537
23. Robinson, B. S., Huang, J., Hong, Y., and Moberg, K. H. (2010) Crumbs regulates Salvador/Warts/Hippo signaling in *Drosophila* via the FERM-domain protein Expanded. *Curr. Biol.* **20,** 582–590
24. Varelas, X., Samavarchi-Tehrani, P., Narimatsu, M., Weiss, A., Cockburn, K., Larsen, B. G., Rossant, J., and Wrana, J. L. (2010) The Crumbs complex couples cell density sensing to Hippo-dependent control of the TGF-β-SMAD pathway. *Dev. Cell* **19,** 831–844
25. Médina, E., Williams, J., Klipfell, E., Zarnescu, D., Thomas, G., and Le Bivic, A. (2002) Crumbs interacts with moesin and β(Heavy)-spectrin in the apical membrane skeleton of *Drosophila*. *J. Cell Biol.* **158,** 941–951
26. Sato, N., Funayama, N., Nagafuchi, A., Yonemura, S., Tsukita, S., and Tsukita, S. (1992) A gene family consisting of ezrin, radixin and moesin. Its specific localization at actin filament/plasma membrane association sites. *J. Cell Sci.* **103,** 131–143
27. Bretscher, A., Edwards, K., and Fehon, R. G. (2002) ERM proteins and merlin: integrators at the cell cortex. *Nat. Rev. Mol. Cell Biol.* **3,** 586–599
28. Fehon, R. G., McClatchey, A. I., and Bretscher, A. (2010) Organizing the cell cortex: the role of ERM proteins. *Nat. Rev. Mol. Cell Biol.* **11,** 276–287
29. Fiévet, B., Louvard, D., and Arpin, M. (2007) ERM proteins in epithelial cell organization and functions. *Biochim. Biophys. Acta* **1773,** 653–660
30. Bretscher, A., Chambers, D., Nguyen, R., and Reczek, D. (2000) ERM-Merlin and EBP50 protein families in plasma membrane organization and function. *Annu. Rev. Cell Dev. Biol.* **16,** 113–143
31. Gould, K. L., Bretscher, A., Esch, F. S., and Hunter, T. (1989) cDNA cloning and sequencing of the protein-tyrosine kinase substrate, ezrin, reveals homology to band 4.1. *EMBO J.* **8,** 4133–4142
32. Lankes, W. T., and Furthmayr, H. (1991) Moesin: a member of the protein 4.1-talin-ezrin family of proteins. *Proc. Natl. Acad. Sci. U.S.A.* **88,** 8297–8301
33. Funayama, N., Nagafuchi, A., Sato, N., Tsukita, S., and Tsukita, S. (1991) Radixin is a novel member of the band 4.1 family. *J. Cell Biol.* **115,** 1039–1048
34. Hirao, M., Sato, N., Kondo, T., Yonemura, S., Monden, M., Sasaki, T., Takai, Y., Tsukita, S., and Tsukita, S. (1996) Regulation mechanism of ERM (ezrin/radixin/moesin) protein/plasma membrane association: possible involvement of phosphatidylinositol turnover and Rho-dependent signaling pathway. *J. Cell Biol.* **135,** 37–51
35. Matsui, T., Maeda, M., Doi, Y., Yonemura, S., Amano, M., Kaibuchi, K., Tsukita, S., and Tsukita, S. (1998) Rho-kinase phosphorylates COOH-terminal threonines of ezrin/radixin/moesin (ERM) proteins and regulates their head-to-tail association. *J. Cell Biol.* **140,** 647–657
36. Simons, P. C., Pietromonaco, S. F., Reczek, D., Bretscher, A., and Elias, L. (1998) C-terminal threonine phosphorylation activates ERM proteins to link the cell's cortical lipid bilayer to the cytoskeleton. *Biochem. Biophys. Res. Commun.* **253,** 561–565
37. Nakamura, F., Huang, L., Pestonjamasp, K., Luna, E. J., and Furthmayr, H. (1999) Regulation of F-actin binding to platelet moesin *in vitro* by both phosphorylation of threonine 558 and polyphosphatidylinositides. *Mol. Biol. Cell* **10,** 2669–2685
38. Delaglio, F., Grzesiek, S., Vuister, G. W., Zhu, G., Pfeifer, J., and Bax, A. (1995) NMRPipe: a multidimensional spectral processing system based on UNIX pipes. *J. Biomol. NMR* **6,** 277–293
39. Otwinowski, Z., and Minor, W. (1997) Processing of x-ray diffraction data collected in oscillation mode. *Methods Enzymol.* **276,** 307–326
40. Adams, P. D., Grosse-Kunstleve, R. W., Hung, L. W., Ioerger, T. R., McCoy, A. J., Moriarty, N. W., Read, R. J., Sacchettini, J. C., Sauter, N. K., and Terwilliger, T. C. (2002) PHENIX: building new software for automated crystallographic structure determination. *Acta Crystallogr. D Biol. Crystallogr.* **58,** 1948–1954
41. Emsley, P., and Cowtan, K. (2004) Coot: model-building tools for molecular graphics. *Acta Crystallogr. D Biol. Crystallogr.* **60,** 2126–2132
42. Davis, I. W., Leaver-Fay, A., Chen, V. B., Block, J. N., Kapral, G. J., Wang, X., Murray, L. W., Arendall, W. B., 3rd, Snoeyink, J., Richardson, J. S., and Richardson, D. C. (2007) MolProbity: all-atom contacts and structure validation for proteins and nucleic acids. *Nucleic Acids Res.* **35,** W375–W383
43. Thompson, J. D., Higgins, D. G., and Gibson, T. J. (1994) ClustalW: improving the sensitivity of progressive multiple sequence alignment through sequence weighting, position-specific gap penalties and weight matrix choice. *Nucleic Acids Res.* **22,** 4673–4680
44. Pearson, M. A., Reczek, D., Bretscher, A., and Karplus, P. A. (2000) Structure of the ERM protein moesin reveals the FERM domain fold masked by an extended actin binding tail domain. *Cell* **101,** 259–270
45. Hamada, K., Shimizu, T., Yonemura, S., Tsukita, S., Tsukita, S., and Hakoshima, T. (2003) Structural basis of adhesion-molecule recognition by ERM proteins revealed by the crystal structure of the radixin-ICAM-2 complex. *EMBO J.* **22,** 502–514
46. Terawaki, S., Kitano, K., and Hakoshima, T. (2007) Structural basis for type II membrane protein binding by ERM proteins revealed by the radixin-neutral endopeptidase 24.11 (NEP) complex. *J. Biol. Chem.* **282,** 19854–19862
47. Takai, Y., Kitano, K., Terawaki, S., Maesaki, R., and Hakoshima, T. (2008) Structural basis of the cytoplasmic tail of adhesion molecule CD43 and its binding to ERM proteins. *J. Mol. Biol.* **381,** 634–644
48. Mori, T., Kitano, K., Terawaki, S., Maesaki, R., Fukami, Y., and Hakoshima, T. (2008) Structural basis for CD44 recognition by ERM proteins. *J. Biol. Chem.* **283,** 29602–29612
49. García-Alvarez, B., de Pereda, J. M., Calderwood, D. A., Ulmer, T. S., Critchley, D., Campbell, I. D., Ginsberg, M. H., and Liddington, R. C. (2003) Structural determinants of integrin recognition by talin. *Mol. Cell* **11,** 49–58
50. Wegener, K. L., Partridge, A. W., Han, J., Pickford, A. R., Liddington, R. C., Ginsberg, M. H., and Campbell, I. D. (2007) Structural basis of integrin activation by talin. *Cell* **128,** 171–182
51. Li, Y., Wei, Z., Zhang, J., Yang, Z., and Zhang, M. (2014) Structural basis of the binding of Merlin FERM domain to the E3 ubiquitin ligase substrate adaptor DCAF1. *J. Biol. Chem.* **289,** 14674–14681
52. Hirano, Y., Hatano, T., Takahashi, A., Toriyama, M., Inagaki, N., and Hakoshima, T. (2011) Structural basis of cargo recognition by the myosin-X MyTH4-FERM domain. *EMBO J.* **30,** 2734–2747
53. Wei, Z., Yan, J., Lu, Q., Pan, L., and Zhang, M. (2011) Cargo recognition mechanism of myosin X revealed by the structure of its tail MyTH4-FERM tandem in complex with the DCC P3 domain. *Proc. Natl. Acad. Sci. U.S.A.* **108,** 3572–3577
54. Hamada, K., Shimizu, T., Matsui, T., Tsukita, S., and Hakoshima, T. (2000) Structural basis of the membrane-targeting and unmasking mechanisms of the radixin FERM domain. *EMBO J.* **19,** 4449–4462
55. Aragona, M., Panciera, T., Manfrin, A., Giulitti, S., Michielin, F., Elvassore, N., Dupont, S., and Piccolo, S. (2013) A mechanical checkpoint controls multicellular growth through YAP/TAZ regulation by actin-processing factors. *Cell* **154,** 1047–1059
56. Dupont, S., Morsut, L., Aragona, M., Enzo, E., Giulitti, S., Cordenonsi, M., Zanconato, F., Le Digabel, J., Forcato, M., Bicciato, S., Elvassore, N., and Piccolo, S. (2011) Role of YAP/TAZ in mechanotransduction. *Nature* **474,** 179–183
57. Sansores-Garcia, L., Bossuyt, W., Wada, K., Yonemura, S., Tao, C., Sasaki, H., and Halder, G. (2011) Modulating F-actin organization induces organ growth by affecting the Hippo pathway. *EMBO J.* **30,** 2325–2335
58. Zhao, B., Li, L., Wang, L., Wang, C. Y., Yu, J., and Guan, K. L. (2012) Cell detachment activates the Hippo pathway via cytoskeleton reorganization to induce anoikis. *Genes Dev.* **26,** 54–68
59. Piccolo, S., Dupont, S., and Cordenonsi, M. (2014) The biology of YAP/TAZ: hippo signaling and beyond. *Physiol. Rev.* **94,** 1287–1312
60. Low, B. C., Pan, C. Q., Shivashankar, G. V., Bershadsky, A., Sudol, M., and Sheetz, M. (2014) YAP/TAZ as mechanosensors and mechanotransducers in regulating organ size and tumor growth. *FEBS Lett.* **588,** 2663–2670

Protein Structure and Folding:

Structural Basis for the Phosphorylation-regulated Interaction between the Cytoplasmic Tail of Cell Polarity Protein Crumbs and the Actin-binding Protein Moesin

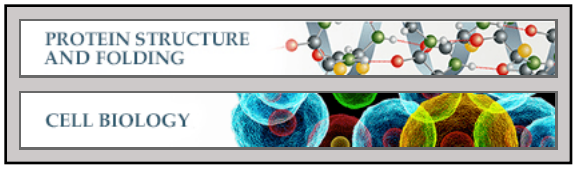

Zhiyi Wei, Youjun Li, Fei Ye and Mingjie Zhang

J. Biol. Chem. 2015, 290:11384-11392.
doi: 10.1074/jbc.M115.643791 originally published online March 19, 2015